Accepted to J. Chem. Phys. 10.1063/5.0139795

Narrow Homogeneous Linewidths and Slow Cooling Dynamics across Infrared Intra-band Transitions in n-Doped HgSe Colloidal Quantum Dots

Ashley M. Stingel[1], Jari Leemans[2], Zeger Hens[2,3], Pieter Geiregat[2,3], and Poul B. Petersen[1*]

1 Physical Chemistry II, Faculty of Chemistry & Biochemistry, Ruhr-University Bochum, Bochum, Germany

2 Physics and Chemistry of Nanostructures Group, Department of Chemistry, Faculty of Sciences, Ghent University, 9000 Gent, Belgium.

3 NoLIMITS Center for Non-Linear Microscopy and Spectroscopy, Ghent University, 9000 Gent, Belgium.

Corresponding author email: poul.petersen@ruhr-uni-bochum.de

Abstract

Intra-band transitions in colloidal quantum dots (QDs) are promising for opto-electronic applications in the mid-IR spectral region. However, such intra-band transitions are typically very broad and spectrally overlapping, making the study of individual excited states and their ultrafast dynamics very challenging. Here, we present a first full spectrum 2D IR (2D CIR) spectroscopy study of intrinsically n-doped HgSe QDs, which exhibit mid-infrared intra-band transitions in their ground state. The obtained 2D CIR spectra reveal that underneath the broad absorption line shape of ~500 cm^{-1}, the transitions exhibit surprisingly narrow intrinsic linewidths with a homogeneous broadening of 175-250 cm^{-1}. Furthermore, the 2D IR spectra are remarkably invariant, with no sign of spectral diffusion dynamics at waiting times up to 50 ps. Accordingly, we attribute the large static inhomogeneous broadening to the distribution of size and doping level of the QDs. In addition, the two higher lying P-states of the QDs can be clearly identified in the 2D IR spectra along the diagonal with a cross-peak. However, there is no indication of cross-peak dynamics indicating that, despite the strong spin-orbit coupling in HgSe, transitions between the P-states must be longer than our maximum waiting time of 50 ps. This study illustrates a new frontier of 2D IR spectroscopy enabling the study of intra-band carrier dynamics in nanocrystalline materials across the entire mid-infrared spectrum.

Introduction

Opto-electronic devices, such as light sources and detectors, in the mid-infrared (IR) spectrum are currently limited and consequently an active area of research and development. Intra-band optical transitions are of particular interest for applications in IR opto-electronics due to their high oscillator strength, leading to strong absorption, efficient fluorescence, and, potentially, light amplification in the mid-IR range. Although common for intra-band quantum cascade lasers, the use of such narrowly spaced transitions based on solution processable semiconductor quantum dots (QDs) remains to date underexplored despite observations of efficient and tunable intra-band absorption and luminescence.[1-7] Several fundamental questions remain unanswered, such as the nature of electron relaxation across higher excited intra-band states, or whether the large absorption and fluorescence linewidths found in IR active QDs are intrinsic or dominated by other factors, such as size dispersion. One reason for these gaps in knowledge is the absence of suitable methods to study the photo-physics across such low energy transitions with the same advanced optical techniques found in the visible spectrum. In particular, the lack of simultaneously broadband and ultrafast time-resolved techniques has been a limiting factor. Since intra-band transitions in QDs are often broadened across several thousand wavenumbers, the need for broadband probing on fast timescales becomes obvious. Simultaneously resolving dynamics across broad and congested spectra on ultrafast scales is nearly impossible due to energy/time resolution restrictions in the mid-IR spectral region. Early attempts to quantify the homogeneous infrared linewidths in nanocrystals were based on hole-burning experiments with a limited spectral coverage.[8] In this regard, full spectrum two-dimensional continuum infrared (2D CIR) spectroscopy could offer a way forward as the method provides simultaneous high frequency and time resolution and offers direct insight into the homogeneous linewidth of transitions. While interband transitions in QDs have been studied with 2D visible spectroscopy,[9-17] intra-band transitions in the mid-IR have so far not been studied with 2D

spectroscopy, mainly since conventional 2D IR spectroscopy does not offer the spectral bandwidth needed to capture the broad intra-band transitions.

Over the last 25 years, 2D IR spectroscopy has developed into a powerful method for measuring the ultrafast vibrational dynamics across a wealth of complex systems such as water, metal-complexes, proteins, and other biological samples.[18-26] 2D IR spectroscopy is often presented as the vibrational analogue of 2D NMR spectroscopy as it can characterize the couplings between transitions, separate homogeneous broadening from the full, inhomogeneously broadened linewidths of complex spectra, quantify spectral diffusion dynamics, and identify timescales for population transfer.[27-29] However, while the complete 2D NMR spectrum can be routinely obtained, thereby characterizing all potential couplings between all spin states, the spectral coverage in 2D IR spectroscopy is typically much more limited due to the narrow bandwidths of infrared OPA sources – typically a few hundred cm^{-1} – corresponding to about 10% of the vibrational spectrum. As a result, using such conventional OPA pulses for both excitation and detection results in capturing about 1% of the potential 2D IR spectrum. Clearly, such coverage falls short of that needed to study broad intra-band transitions in colloidal QDs, which can span more than 1000 cm^{-1}, as shown in the linear FTIR spectrum of n-doped HgSe QDs in Figure 1. In recent years, continuum pulses spanning the whole mid-IR spectral range (~1000 – 4000 cm^{-1}) have been generated[30, 31] and incorporated as probe pulses in ultrafast transient and 2D IR experiments.[32-36] While these continuum mid-IR pulses are currently too weak to efficiently excite molecular vibrations, they are strong enough to excite high oscillator strength electronic states in semiconductors. Stingel *et al.* recently demonstrated the first implementation of continuum infrared pulses for both excitation and detection in 2D IR experiments to obtain 2D CIR surfaces of bulk semiconductors.[37] In this study, we apply this 2D CIR method to the intra-band transitions in intrinsically doped HgSe QDs to unravel the nature of line broadening and excited state transitions.

In particular, we investigated 5.5 nm HgSe QDs capped with oleylamine (OLA) ligands, synthesized according to a modified procedure from Deng *et al*.[38, 39] The FTIR spectrum of the QDs in their ground state is displayed in Figure 1a. The doping of the conduction band results in a collapse of the lowest lying interband transition from the valence S-state to the conduction band S-state and a concomitant surge of the intra-band $1S_e$-$1P_e$ transition band in the mid-infrared. Based on this and the 2-fold degeneracy of the $1S_e$ conduction band state, we calculate that the HgSe QDs in the present study have an average doping level of 1.9 electrons per QD. Accordingly, the doubly doped QD is the most prominent within the sample ensemble. From this $1S_e$-state, the electrons can be excited to the $1P_{1/2}$ and $1P_{3/2}$ states, as illustrated in Figure 1b. The P-states are split because of spin-orbit coupling and shape asymmetry, as shown by Hudson *et al.*[40] The observed spectrum results from these two broad and overlapping transitions from the S-state to each of the P-states, which can be fit with two broad Gaussians. In addition to these broad intra-band transitions, the FTIR spectrum displays sharp CH vibrations from the organic ligands around 2900 cm^{-1}. The broad intra-band transition linewidth of ~500 cm^{-1} for each P-state should result from both homogeneous broadening and a sizable inhomogeneous broadening due to the size distribution within the sample ensemble, leading to varying transition energies and doping levels. Furthermore, the transition rate between the P-states has not been determined exactly despite claims of slow relaxation on the 5 to 30 ps timescale, based on modeling of picosecond fluorescence experiments.[41] Conventional ultrafast transient mid-IR absorption experiments of similar HgS QDs were previously performed to map out the relaxation times and multicarrier dynamics, over a comparatively narrow range of probing.[42] In this study we perform full spectrum 2D CIR spectroscopy to characterize the homogeneous and inhomogeneous broadening of these HgSe QDs and set a lower limit to the relaxation time between the P-states to 50 ps.

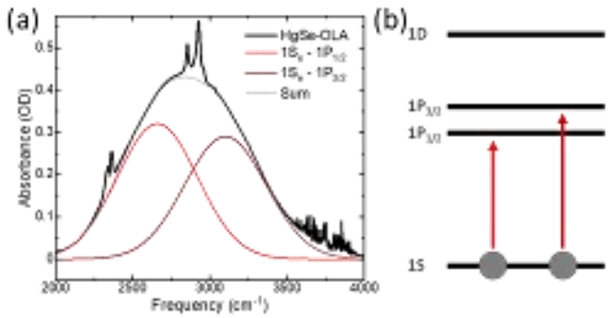

Figure 1: (a) Linear FTIR spectrum of n-doped HgSe QDs with OLA ligands with a model of the two contributing transitions from the $1S_e$ to $1P_{1/2}$ and $1P_{3/2}$ states. The CH stretches from the ligands are seen at ~2900 cm^{-1}, while atmospheric absorbances from CO_2 and water vapor appear in the spectrum at 2350 and above 3500 cm^{-1}, respectively. (b) A schematic of the conduction band level diagram, illustrating the mid-IR intra-band transitions observed in the FTIR spectrum.

Methods

Full Spectrum 2D IR Spectroscopy. The experimental setup for 2D CIR spectroscopy has been described previously for the application of bulk InAs.[37] Briefly, 1.3 mJ of the output from a 25 fs, Ti:sapphire laser system is used to generate mid-IR continuum pulses via the filamentation of the first, second, and third harmonics in air. The mid-IR continuum is separated from the driving wavelengths with a silicon filter and divided into the pump and probe paths with a 50:50 KBr beamsplitter. The pump is further divided into multiple pulses in a Mach-Zehnder interferometer, and the resulting pump pair is overlapped with the probe at the sample. Due to the broad bandwidth of the intra-band transitions, the detection axis was measured over 2-3 monochromator positions and detected by a 128-by-128 pixel MCT focal plane array (PhaseTech, 2DMCT). The spectrometer is equipped with order-sorting filters to block higher diffraction orders.

Synthesis of HgSe QDs

HgSe quantum dots (QDs) with oleylamine (OLA) ligands were synthesized based on the procedure published by Deng *et al.*[38, 39] Additional synthesis details are provided in the supporting information. The HgSe QDs were solvated in tetrachloroethylene and contained in a sandwich-type sample cell with a 200

μm thick PTFE spacer contained between 1 mm thick CaF_2 windows. While two samples with average dot sizes of 5.5 and 4.5 nm were prepared and studied with full spectrum 2D CIR, the analysis discussed here focuses primarily on the larger sample. The FTIR spectra of both samples are shown in the supporting information in Figure S1.

Results

Description of the 2D IR spectrum

Figure 2a displays a 2D CIR surface at a waiting time of 5 ps. Upon excitation, the HgSe QDs exhibit a broad bleach feature from the reduced S-to-P transitions and a smaller induced absorbance at lower frequencies, most likely due to the combination of transitions from the P to the D states and/or possible biexciton shifts of the P-states. A diagram of the electronic states of the QDs and their contributions to the 2D surface is shown in Figure 2b. An artifact around the CO_2 stretch vibrations occurs at the edge of the spectrum (~2350 cm^{-1}) due to imperfect purging and complicates analysis of this region. The 2D CIR spectrum is highly elongated along the diagonal, indicating a large inhomogeneity in the spectrum.[27]

Furthermore, the two separate P-states can be identified in the 2D IR spectrum with a weak cross-peak. In the more common 2D IR spectroscopy of vibrations, separate modes can either be coupled or uncoupled. Coupled vibrational modes give rise to cross-peaks that result from the anharmonic shift of the combination band with respect to the sum of the individual fundamental vibrational frequencies. For uncoupled modes, there is no anharmonic shift for the combination band and, correspondingly, no cross-peak. In the present case, the observed cross-peak does not necessarily indicate that the P-states in different spin-states are coupled, but rather that the electrons share the common $1S_e$ ground state. In the case of carriers in semiconductor QDs, exciting one transition will always cause a bleach in the other transition since the excitation of either reduces the population in the common ground state, as illustrated

in Figure 2b. Here, stimulated emission will also contribute to the overall signal, which gives rise to a moderate cross-peak intensity and a strong bleach on the diagonal.

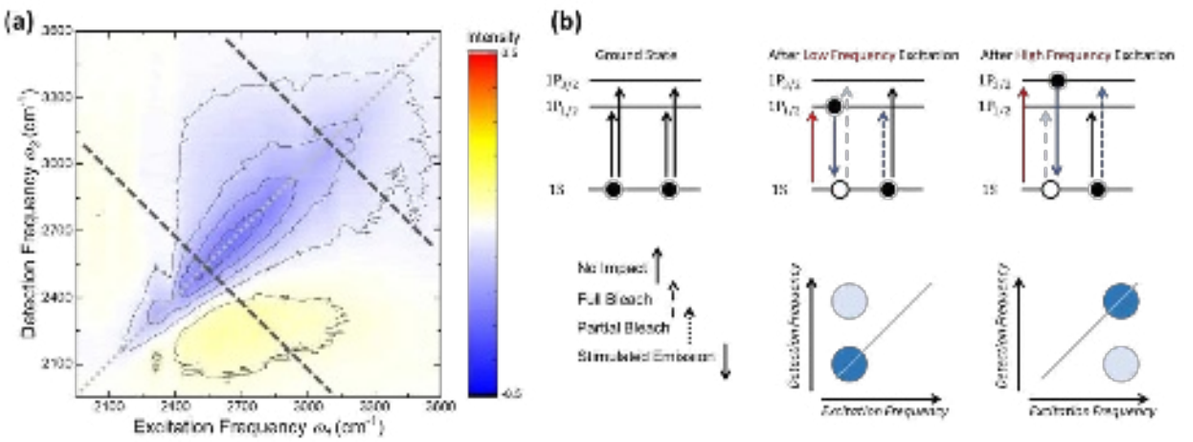

Figure 2: (a) Full spectrum 2D CIR surface of HgSe-OLA QDs at a waiting time t_2=5 ps and (b) a schematic of the transitions contributing to the observed negative (blue) responses. The dotted lines in 2a designate the diagonal and anti-diagonal cuts at the peaks of each P-state transition at approximately 2600 and 3100 cm^{-1}, which are presented in Figure 3.

Linewidths and Spectral Diffusion

As previously discussed, 2D IR spectroscopy can resolve the homogeneous linewidth from the total linewidth, which includes inhomogeneous broadening that results from the distribution of physical sizes and doping levels within the sample ensemble. The total and homogeneous linewidths are quantified from the diagonal and anti-diagonal slices, centered at each of the two P transitions, of the 2D CIR spectrum respectively, as illustrated by the dotted lines in Figure 2 and shown in Figure 3.

In the linear FTIR spectrum, the two P-states are overlapping and difficult to distinguish. The diagonal slice of the 2D spectrum, where the two P-states are better resolved than in the FTIR spectrum, is fit with two Gaussian peaks, yielding the total linewidth for each P-state. The fit of the diagonal slice of the 2D surface at 5 ps is shown in Figure 3a and results in two Gaussians profiles with center frequencies

at approximately 2600 and 3100 cm^{-1}, and widths of about 500 cm^{-1}, in agreement with the FTIR analysis of Figure 1. The higher frequency peak appears narrower in the 2D spectrum than in the FTIR due to the spectral brightness of the pump, which decreases above 3000 cm^{-1}.

The anti-diagonal at the center frequency of each of the two P-states identified above is then fit with a Lorentzian peak to obtain the homogeneous linewidth for each. For the 2D surface at 5 ps, these are shown in Figures 3c and 3d. The anti-diagonal slices are nearly perfectly Lorentzian, which indicate that this linewidth is purely homogeneous in nature. The $1S_e$-$1P_{1/2}$ peak fit underestimates the true width of the peak due to the overlapping induced absorbance peak. This width sets a minimum value for the homogeneous linewidth. The observed homogeneous broadening is likely resulting from ultrafast, sub-picosecond, dephasing caused by phonon scattering that is typical for crystalline semiconductors.[43] Here the homogeneous linewidths are found to be about 150 and 250 cm^{-1}, narrower than the full linewidth of 550 cm^{-1} by a factor of more than a factor of 2. This indicates that narrow intra-band linewidths are intrinsically possible upon further refinement of the synthesis and/or size purification, making n-doped QDs promising candidates for opto-electronic applications in the mid-IR spectral range.

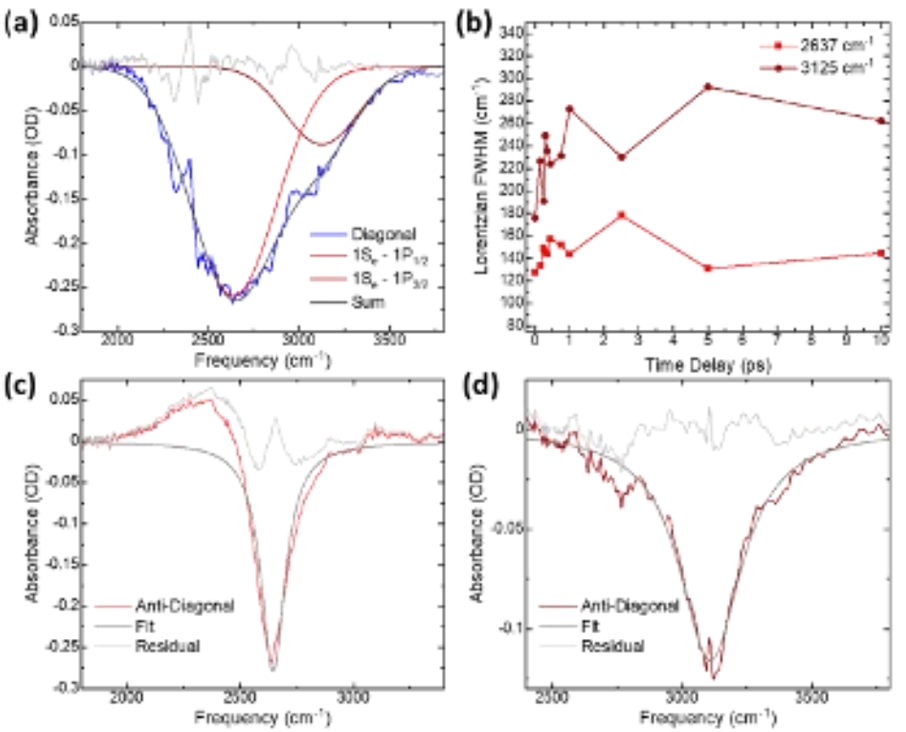

Figure 3: (a) The diagonal cut of the 2D surface at t_2=5 ps fit with two Gaussian profiles, representing the two S-to-P transitions. (b) The homogeneous linewidths of the two P-states as a function of the waiting time, determined from Lorentzian fits of the antidiagonal cuts at the center frequencies of each state. The antidiagonal cut and fits from the t_2=5ps surface are shown for (c) the $1S_e$-$1P_{1/2}$ and (d) the $1S_e$-$1P_{3/2}$ transitions.

To characterize any potential spectral diffusion dynamics, we performed a waiting-time series. Select waiting times are shown in Figure 4, with additional waiting times included in the supporting information in Figure S2. The most striking feature of this waiting-time series is that the 2D IR spectra appear static with negligible changes as a function of the waiting time, except for the trivial overall intensity decrease due to population relaxation. Vibrational modes typically show a fast, picosecond, dynamic inhomogeneity resulting from fast solvent motion, which can make the anti-diagonal slices evolve to non-Lorentzian shapes over time. This is not observed for the QDs, showing that the electronic energy levels in the core of the QDs are not affected by fast solvent or ligand motions. The static nature of the 2D

surface is also captured in the waiting time dependence of the anti-diagonal width shown in Figure 3b. Very little change in the anti-diagonal linewidth is observed. This complete absence of spectral diffusion dynamics on molecular vibrational timescales means that the electronic energy levels of the QDs are isolated from solvent and ligand motions. This is not trivial given the close spectral overlap between the ligand and solvent vibrational modes and the electronic QD transitions. In summary, the spectra are dominated by the static inhomogeneous broadening due to the nanocrystal size and doping level dispersion within the sample ensemble. Such observations are in line with studies on the near-infrared interband transition in PbS QDs by Park *et al*.[16] and on visible interband transitions in CdSe.[14] The ligand shell vibrational dynamics do not influence the linewidth, ensuring colloidally dispersed infrared materials can still show narrow linewidths.

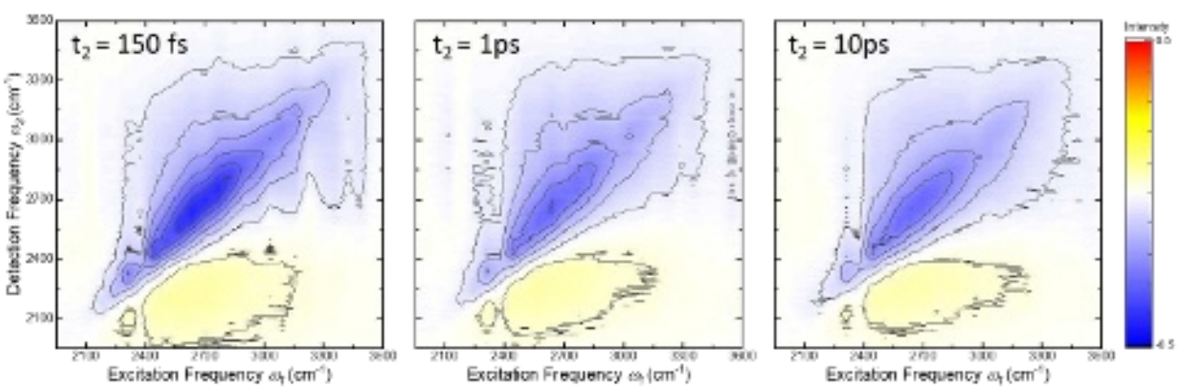

Figure 4: Select 2D CIR surfaces of HgSe-OLA QDs, showing little change over waiting times up to 10 ps. Additional waiting times are shown in Figure S2 in the supporting information.

An additional sample, with a slightly smaller average size, was studied up to a waiting time of 50 ps, shown in Figure S3 in the supporting information. Other than a small frequency shift in the linear spectrum, due to the smaller average size, the results are consistent.

Cross-Peaks

Given the split nature of the P-manifold, we would expect population relaxation dynamics between the P-states. If an electron is occupying the higher lying 4-fold degenerate $1P_{3/2}$ state, it should be able to relax down to the 2-fold degenerate $1P_{1/2}$ state by dissipating its energy and flipping its spin. However, a close look at the 2D waiting series shown in Figure 4 and Figure S3 shows no indication that the cross-peak intensity between the two P-states increases over time, even up to a waiting time of 50 ps. This shows that any transition time between the two P-states is at least slower than 50 ps. This result is surprising given that the nanocrystals are composed of the heavy-element Hg, which typically induces a strong spin-orbit coupling leading to spin flips and relaxation between the two states. Reports based on ultrafast luminescence experiments with a ca. 10 ps time resolution indicated a similar remarkably slow intra-P state relaxation in-line with our observations.[41] In addition to the spin-flip, energy conservation is required implying that the energy of the electron needs to be dissipated to either phonons,[44-47] ligand vibrations or, via Auger coupling to an empty hole level.[48, 49] The latter mechanism is highly unlikely as the valence band is fully occupied in HgSe and the 'hole' in the isolated 1S level has no free energy levels to occupy at higher hole energy.[41] Low-frequency ligand vibrations, occurring at frequencies around 500 cm^{-1}, could play a role but are difficult to estimate. A typical phonon in HgSe has an energy of 150 cm^{-1}, implying multiple phonons need to be emitted simultaneously – typically considered an unlikely process.[50]

Conclusion

We have acquired full spectrum 2D CIR spectra of the intra-conduction band transitions of intrinsically n-doped HgSe QDs. The 2D CIR spectra reveal a narrow intra-band homogeneous linewidth of ~200 cm^{-1}, indicating that the broad total linewidth is mainly due to the static inhomogeneous size and doping-level distribution within the ensemble. This observation implies that further refinement of QD synthesis and/or

purification can dramatically reduce the infrared optical linewidth of doped nanocrystals. Furthermore, the two split P-states are identified in the 2D spectrum with a clear cross-peak due to a common ground state. However, no change in the cross-peak intensity as indicative of population transfer is noticeable up to a 50 ps waiting time, thereby setting a lower bound to the timescale of the transition between the singlet and triplet P-states. This shows that spin is a conserved quantum number in these nanocrystals despite being composed of Hg. Our study illustrates that full spectrum 2D CIR spectroscopy can provide valuable information about carrier properties and optical transitions in infrared active semiconductors, such as colloidal QDs, that currently cannot be obtained by any other means. The present 2D CIR experiments of doped QDs, which exhibit intra-band transitions in their electronic ground state, can be extended to virtually any QD in transient (visible or NIR pump) – 2D CIR experiments. Such experiments can probe the intra-band transitions and dynamics of conduction band electrons and potentially also the valence band holes of the photoinduced excitons. Alternatively, the CIR pulses can be incorporated in mixed visible/NIR and CIR experiments in 2DEV or transient 2DVE to probe the couplings between the inter- and intra-band transitions. In such experiments, the full spectral coverage in the mid-IR by the CIR pulse to critical to resolve the intraband transitions. The present study thus establishes a new and exciting frontier for 2D IR spectroscopy.

SUPPLEMENTARY MATERIAL

See Supplementary Material for further details on the HgSe QD synthesis, additional experimental details on the two HgSe samples, and additional 2D CIR spectra.

ACKNOWLEDGMENTS

Funded by the Deutsche Forschungsgemeinschaft (DFG, German Research Foundation) under Germany's Excellence Strategy - EXC 2033 - 390677874 – RESOLV.

AUTHOR DECLARATIONS

The authors have no conflicts to disclose.

Author Contributions

Ashley M. Stingel: Conceptualization (Lead), Data Curation (Lead), Formal Analysis (Lead), Investigation (Lead), Methodology (Equal), Software (Lead), Validation (Lead), Visualization (Equal), Writing/Original Draft Preparation (Equal), Writing/Review and Editing (Equal);

Jari Leemans: Methodology (Equal), Writing/Review & Editing (Supporting);

Zeger Hens: Conceptualization (Supporting), Funding Acquisition (Supporting), Methodology (Equal), Resources (Equal), Writing/Review & Editing (Supporting);

Pieter Geiregat: Conceptualization (Supporting), Funding Acquisition (Supporting), Methodology (Equal), Resources (Equal), Supervision (Equal), Visualization (Equal), Writing/Original Draft Preparation (Equal), Writing/Review & Editing (Equal);

Poul B. Petersen: Conceptualization (Supporting), Data Curation (Supporting), Funding Acquisition (Lead), Methodology (Equal), Project Administration (Lead), Resources (Equal), Supervision (Equal), Writing/Original Draft Preparation (Equal), Writing/Review & Editing (Equal)

REFERENCES

1. C. Livache, B. Martinez, N. Goubet, C. Gréboval, J. Qu, A. Chu, S. Royer, S. Ithurria, M. G. Silly, B. Dubertret and E. Lhuillier, Nature Communications **10** (1) (2019).
2. Z. Deng, K. S. Jeong and P. Guyot-Sionnest, ACS Nano **8** (11), 11707-11714 (2014).
3. X. Shen, J. C. Peterson and P. Guyot-Sionnest, ACS Nano **16** (5), 7301-7308 (2022).
4. J. Qu, M. Weis, E. Izquierdo, S. G. Mizrahi, A. Chu, C. Dabard, C. Gréboval, E. Bossavit, Y. Prado, E. Péronne, S. Ithurria, G. Patriarche, M. G. Silly, G. Vincent, D. Boschetto and E. Lhuillier, Nature Photonics **16** (1), 38-44 (2022).

5. A. Kamath, C. Melnychuk and P. Guyot-Sionnest, Journal of the American Chemical Society **143** (46), 19567-19575 (2021).
6. C. Greboval, A. Chu, N. Goubet, C. Livache, S. Ithurria and E. Lhuillier, Chemical Reviews **121** (7), 3627-3700 (2021).
7. E. Tournié and L. Cerutti, *Mid-infrared optoelectronics : materials, devices, and applications*. (Woodhead Publishing is an imprint of Elsevier, Duxford, United Kingdom ; Cambridge, MA, United States, 2020).
8. M. Shim and P. Guyot-Sionnest, Physical Review B **64** (24) (2001).
9. E. Cassette, J. C. Dean and G. D. Scholes, Small **12** (16), 2234-2244 (2016).
10. W. Zhao, Z. Qin, C. Zhang, G. Wang, X. Huang, B. Li, X. Dai and M. Xiao, The Journal of Physical Chemistry Letters **10** (6), 1251-1258 (2019).
11. T. Stoll, F. Branchi, J. Réhault, F. Scotognella, F. Tassone, I. Kriegel and G. Cerullo, The Journal of Physical Chemistry Letters **8** (10), 2285-2290 (2017).
12. J. M. Richter, F. Branchi, F. Valduga De Almeida Camargo, B. Zhao, R. H. Friend, G. Cerullo and F. Deschler, Nature Communications **8** (1) (2017).
13. E. Cassette, S. Pedetti, B. Mahler, S. Ithurria, B. Dubertret and G. D. Scholes, Physical Chemistry Chemical Physics **19** (12), 8373-8379 (2017).
14. H. Seiler, S. Palato and P. Kambhampati, The Journal of Chemical Physics **149** (7), 074702 (2018).
15. S. Palato, H. Seiler, P. Nijjar, O. Prezhdo and P. Kambhampati, Proceedings of the National Academy of Sciences **117** (22), 11940-11946 (2020).
16. S. D. Park, D. Baranov, J. Ryu, B. Cho, A. Halder, S. Seifert, S. Vajda and D. M. Jonas, Nano Letters **17** (2), 762-771 (2017).
17. G. B. Griffin, S. Ithurria, D. S. Dolzhnikov, A. Linkin, D. V. Talapin and G. S. Engel, The Journal of Chemical Physics **138** (1), 014705 (2013).
18. S. T. Roberts, K. Ramasesha and A. Tokmakoff, Accounts of Chemical Research **42** (9), 1239-1249 (2009).
19. D. E. Moilanen, D. Wong, D. E. Rosenfeld, E. E. Fenn and M. D. Fayer, Proceedings of the National Academy of Sciences **106** (2), 375-380 (2009).
20. C. R. Baiz, P. L. Mcrobbie, J. M. Anna, E. Geva and K. J. Kubarych, Accounts of Chemical Research **42** (9), 1395-1404 (2009).
21. J. P. Kraack, D. Lotti and P. Hamm, The Journal of Chemical Physics **142** (21), 212413 (2015).
22. Z. Ganim, H. S. Chung, A. W. Smith, L. P. Deflores, K. C. Jones and A. Tokmakoff, Accounts of Chemical Research **41** (3), 432-441 (2008).
23. A. Ghosh, J. S. Ostrander and M. T. Zanni, Chemical Reviews **117** (16), 10726-10759 (2017).
24. A. T. Krummel and M. T. Zanni, The Journal of Physical Chemistry B **110** (28), 13991-14000 (2006).
25. Ł. Szyc, M. Yang, E. T. J. Nibbering and T. Elsaesser, Angewandte Chemie International Edition **49** (21), 3598-3610 (2010).
26. J. Zheng, K. Kwak and M. D. Fayer, Accounts of Chemical Research **40** (1), 75-83 (2007).
27. P. Hamm and M. T. Zanni, *Concepts and methods of 2d infrared spectroscopy*. (Cambridge University Pres, Cambridge ; New York, 2011).
28. M. D. Fayer, *Ultrafast infrared and Raman spectroscopy*. (Marcel Dekker, New York, 2001).
29. M. Cho, Chemical Reviews **108** (4), 1331-1418 (2008).
30. P. B. Petersen and A. Tokmakoff, Optics Letters **35** (12), 1962 (2010).
31. C. Calabrese, A. M. Stingel, L. Shen and P. B. Petersen, Opt Lett **37** (12), 2265-2267 (2012).
32. A. M. Stingel and P. B. Petersen, The Journal of Physical Chemistry B **120** (41), 10768-10779 (2016).
33. M. Thamer, L. De Marco, K. Ramasesha, A. Mandal and A. Tokmakoff, Science **350** (6256), 78-82 (2015).
34. J. D. Gaynor, T. L. Courtney, M. Balasubramanian and M. Khalil, Optics Letters **41** (12), 2895 (2016).

35. A. M. Stingel, C. Calabrese and P. B. Petersen, The Journal of Physical Chemistry B **117** (49), 15714-15719 (2013).
36. L. De Marco, K. Ramasesha and A. Tokmakoff, The Journal of Physical Chemistry B **117** (49), 15319-15327 (2013).
37. A. M. Stingel and P. B. Petersen, The Journal of Chemical Physics **155** (10), 104202 (2021).
38. Z. Deng and P. Guyot-Sionnest, ACS Nano **10** (2), 2121-2127 (2016).
39. L. K. Sagar, W. Walravens, J. Maes, P. Geiregat and Z. Hens, The Journal of Physical Chemistry C **121** (25), 13816-13822 (2017).
40. M. H. Hudson, M. Chen, V. Kamysbayev, E. M. Janke, X. Lan, G. Allan, C. Delerue, B. Lee, P. Guyot-Sionnest and D. V. Talapin, ACS Nano **12** (9), 9397-9404 (2018).
41. C. Melnychuk and P. Guyot-Sionnest, ACS Nano **13** (9), 10512-10519 (2019).
42. J. Lim, Y. C. Choi, D. Choi, I. Y. Chang, K. Hyeon-Deuk, K. S. Jeong, K. Kwak and M. Cho, Matter-Us **4** (3), 1072-1086 (2021).
43. J. De Roo, N. Yazdani, E. Drijvers, A. Lauria, J. Maes, J. S. Owen, I. Van Driessche, M. Niederberger, V. Wood, J. C. Martins, I. Infante and Z. Hens, Chemistry of Materials **30** (15), 5485-5492 (2018).
44. D. Bozyigit, N. Yazdani, M. Yarema, O. Yarema, W. M. M. Lin, S. Volk, K. Vuttivorakulchai, M. Luisier, F. Juranyi and V. Wood, Nature **531** (7596), 618-622 (2016).
45. S. C. Boehme, S. T. Brinck, J. Maes, N. Yazdani, F. Zapata, K. Chen, V. Wood, J. M. Hodgkiss, Z. Hens, P. Geiregat and I. Infante, Nano Letters **20** (3), 1819-1829 (2020).
46. A. Pandey and P. Guyot-Sionnest, Science **322** (5903), 929-932 (2008).
47. R. R. Cooney, S. L. Sewall, K. E. H. Anderson, E. A. Dias and P. Kambhampati, Physical Review Letters **98** (17) (2007).
48. J. M. Pietryga, Y.-S. Park, J. Lim, A. F. Fidler, W. K. Bae, S. Brovelli and V. I. Klimov, Chemical Reviews **116** (18), 10513-10622 (2016).
49. V. I. Klimov, The Journal of Physical Chemistry B **104** (26), 6112-6123 (2000).
50. H. Kepa, T. Giebultowicz, B. Buras, B. Lebech and K. Clausen, Phys Scripta **25** (6), 807-809 (1982).

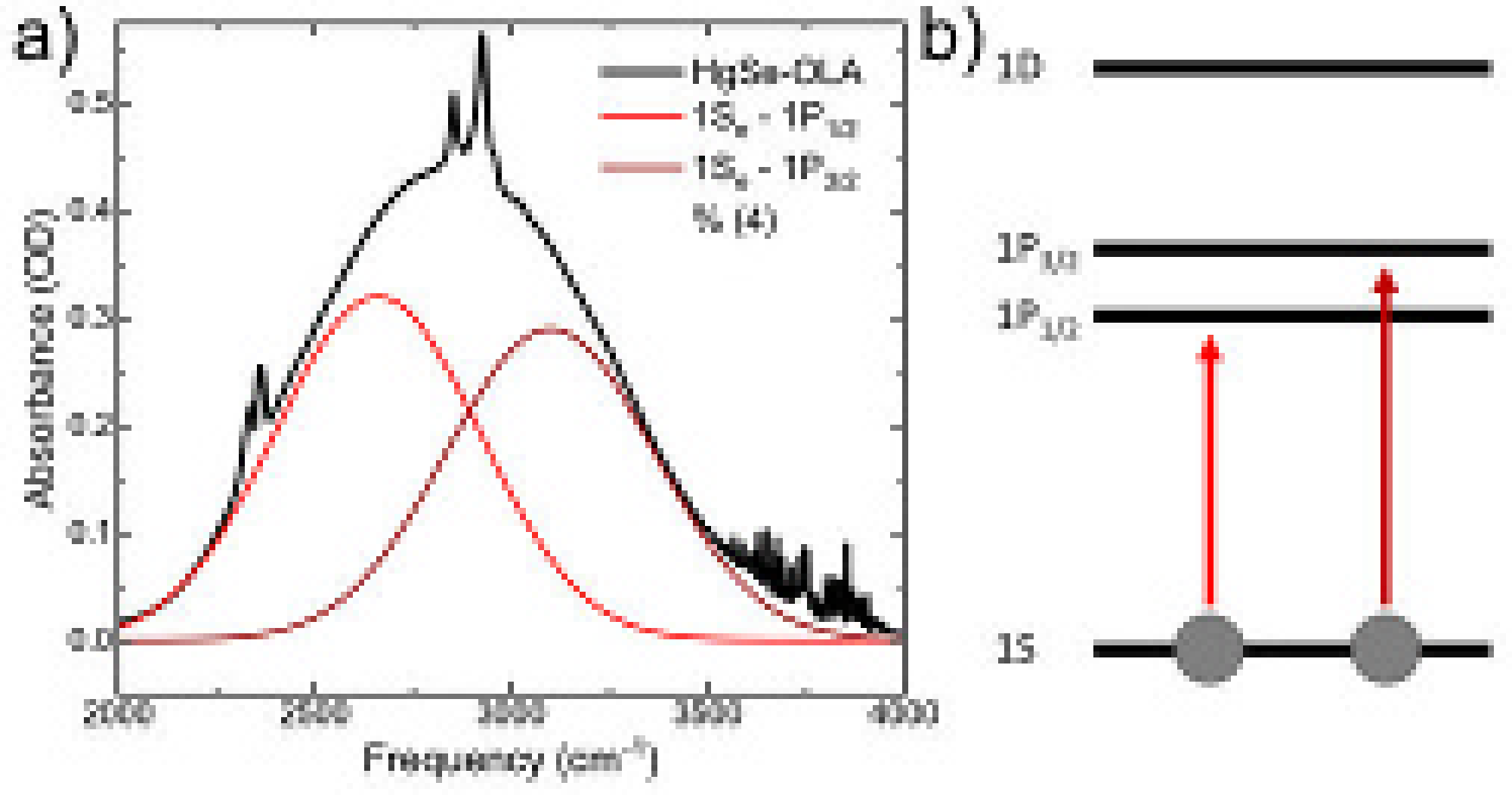
a)
HgSe-OLA
1S$_e$ - 1P$_{1/2}$
1S$_e$ - 1P$_{3/2}$
% (4)
Absorbance (OD)
0.5
0.4
0.3
0.2
0.1
0.0
2000
2500
3000
3500
4000
Frequency (cm^{-1})
b)
1D
1P$_{1/2}$
1P$_{3/2}$
1S

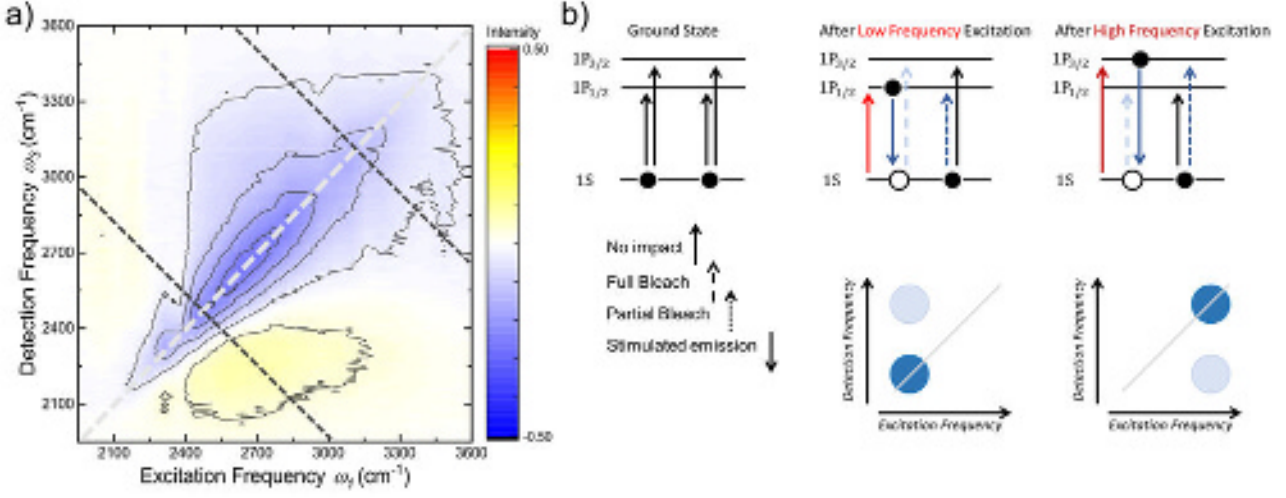
a)
Intensity
0.90
-0.50
Detection Frequency ω_3 (cm^{-1})
Excitation Frequency ω_1 (cm^{-1})
2100
2400
2700
3000
3300
3600
b)
Ground State
$1P_{3/2}$
$1P_{1/2}$
1S
After Low Frequency Excitation
After High Frequency Excitation
No impact
Full Bleach
Partial Bleach
Stimulated emission
Detection Frequency
Excitation Frequency

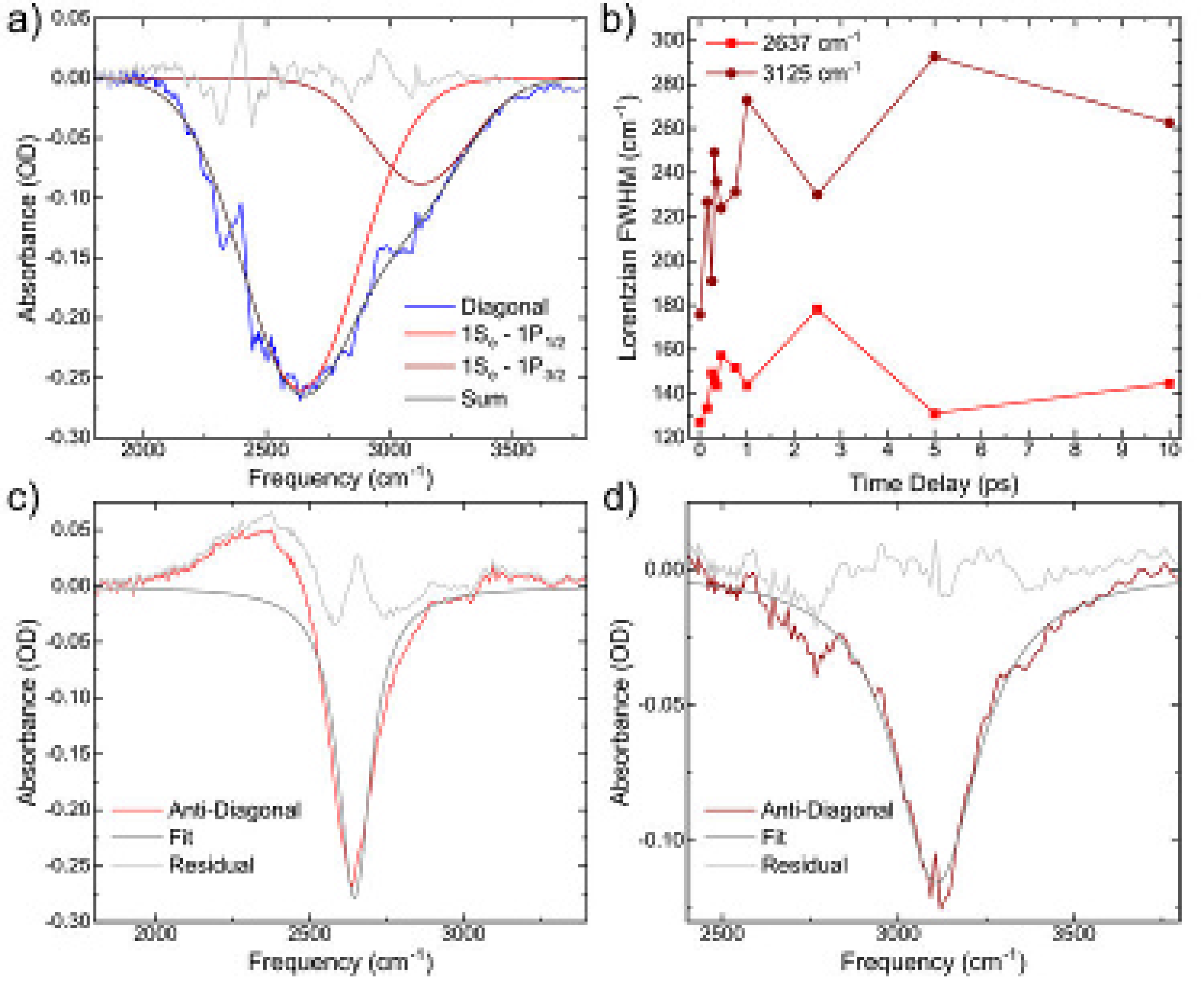
a)
Absorbance (OD)
Frequency (cm^{-1})
Diagonal
$1S_0$ - $1P_{1/2}$
$1S_0$ - $1P_{3/2}$
Sum
b)
Lorentzian FWHM (cm^{-1})
Time Delay (ps)
2637 cm^{-1}
3125 cm^{-1}
c)
Absorbance (OD)
Frequency (cm^{-1})
Anti-Diagonal
Fit
Residual
d)
Absorbance (OD)
Frequency (cm^{-1})
Anti-Diagonal
Fit
Residual

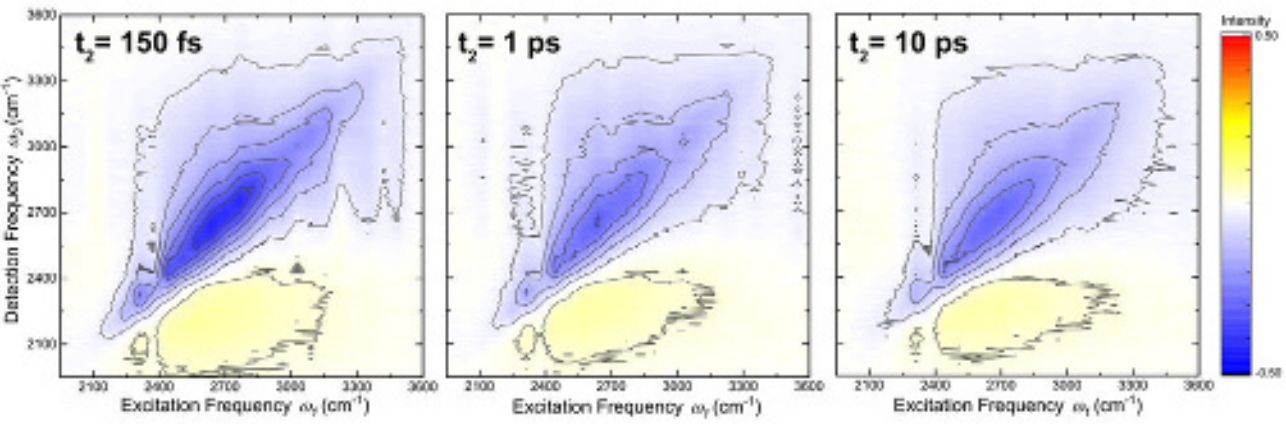
t2= 150 fs
t2= 1 ps
t2= 10 ps
Detection Frequency ω3 (cm-1)
Excitation Frequency ω1 (cm-1)
Excitation Frequency ω1 (cm-1)
Excitation Frequency ω1 (cm-1)
Intensity
0.50
0.00
2100
2400
2700
3000
3300
3600